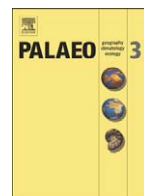




Contents lists available at ScienceDirect

Palaeogeography, Palaeoclimatology, Palaeoecology

journal homepage: www.elsevier.com/locate/palaeo

Quaternary paleoenvironments and relative sea-level changes in Marajó Island (Northern Brazil): Facies, $\delta^{13}\text{C}$, $\delta^{15}\text{N}$ and C/N

Maria Carolina Da Cruz Miranda ^a, Dilce De Fátima Rossetti ^{b,*}, Luiz Carolos Ruiz Pessenda ^c

^a Universidade de São Paulo-USP, Instituto de Geociências, Rua do Lago, 562, 05508-080 São Paulo, SP, Brazil

^b Instituto Nacional de Pesquisas Espaciais-INPE, Rua dos Astronautas 1758-CP 515, 12245-970 São José dos Campos-SP, Brazil

^c Universidade de São Paulo, Laboratório de ^{14}C , Avenida Centenário 303, 13416000 Piracicaba, SP – Brazil

ARTICLE INFO

Article history:

Received 17 December 2008

Received in revised form 31 July 2009

Accepted 6 August 2009

Available online xxx

Keywords:

Sedimentary facies

Carbon and nitrogen isotopes

Relative sea level

Tectonics

Estuary

Late Quaternary

ABSTRACT

The reconstruction of physical environments of Amazonian areas is of great interest to determine the dynamic evolution of the Amazon drainage basin. However, few studies have emphasized the Quaternary deposits in this region, which is mostly due to the lack of natural exposures imposed by the low topography. This work integrates facies analysis, radiocarbon dating, $\delta^{13}\text{C}$, $\delta^{15}\text{N}$, and C/N of an 124 m-thick core from an area located at the mouth of the Amazon River, northeastern Amazonia. The study records deposits up to 50,795 ^{14}C yr B.P. in age, which formed in a variety of depositional environments including fluvial channel, tidal flat, outer estuarine basin to shallow marine, inner estuarine basin, estuarine channel and lagoon. Facies interpretation was significantly improved with the inclusion of $\delta^{13}\text{C}$, $\delta^{15}\text{N}$, and C/N analyses of organic matter extracted from the sediments. The obtained values conform to a transitional, mostly estuarine paleosetting evolved during successive relative sea-level fluctuations. The results suggest fluvial deposition between 40,950 (± 590) and 50,795 ^{14}C yr B.P., with a rise in relative sea level that commenced between 35,567 (± 649) and 39,079 (± 1114) ^{14}C yr B.P. An overall transgression took place until 29,340 (± 340) ^{14}C yr B.P., after which the relative sea level dropped, favoring valley rejuvenation and incision. Following this time up to 10,479 (± 34) ^{14}C yr B.P., a rise in relative sea level filled up the valley with estuarine deposits. After 10,479 (± 34) ^{14}C yr B.P., the estuary was replaced by a lagoon. At the end of the Holocene, the coastline prograded approximately 45 km northward, replacing the lagoon by a lake system. Despite the influence of eustatic fluctuations, regional tectonics played a significant role to create new space where these Late Pleistocene and Holocene sediments accumulated.

© 2009 Elsevier B.V. All rights reserved.

1. Introduction

Late Quaternary sediments in the Brazilian Amazonia lack widespread documentation, despite their great interest for reconstructing changes in the physical environment prior to the modern landscape development. Deposits of this age are prevalent in the shallow subsurface of eastern Marajó Island, located at the mouth of the Amazon River. Geomorphological studies based on remote sensing, combined with regional sedimentological field data, revealed that this area was influenced by a large estuarine system in the late Quaternary (Rossetti et al., 2008a,b). Understanding the origin and evolution of this paleoestuary has large implications for reconstructing both the paleogeography and the history of relative sea-level changes in northern Brazil. Recent researches (Rossetti et al., 2007, 2008a,b) revealed that the Marajó paleoestuary was active until the Pleistocene–Holocene boundary, when the island was detached from the mainland due to the reactivation of tectonic faults. In addition to morphological studies, the characterization of this paleoestuary is only based on sedimentary facies

analysis of core data, because natural exposures are scarce in this region. This approach has limitations when reconstructing depositional environments, because some important facies parameters, such as geometry and lateral facies variations, cannot be observed.

This study focuses on an 124 m-thick core from the eastern margin of the Marajó paleoestuary. Facies interpretation is combined with $\delta^{13}\text{C}$, $\delta^{15}\text{N}$, and C/N analyses of the organic matter preserved in the sediments. Stable isotopic and geochemical analyses may significantly improve sedimentological interpretations, as they provide information on sources and relative quantities of organic material in the depositional systems. $\delta^{13}\text{C}$ analysis of deposited organic matter (e.g., Prahl et al., 1980; Premuzic et al., 1982; Ishiwatari and Usaki, 1987; Jasper and Gagosian, 1990; Meyers, 1994; Prahl et al., 1994; Sifeddine et al., 2001) is used here to determine changes in relative concentration of C_3 and C_4 terrestrial and aquatic vegetations to the organic matter pool in the paleoestuary over time. The isotopic signature of organic matter is composed of an exchange between biochemically incorporated and inorganic carbon available in the atmosphere ($\delta^{13}\text{C} = -7.0\%$) and ocean ($\delta^{13}\text{C} = 0\%$). Thus, C_3 and C_4 land plants show $\delta^{13}\text{C}$ values between -33.0% and -23.0% , and -15.0% and -9.0% , respectively (Deines, 1980). These values are the $\delta^{13}\text{C} = -20.0\%$ and -7.0% of biochemically incorporated carbon from C_3 and C_4 plants, respectively, combined with the $\delta^{13}\text{C} = -7.0\%$ from atmospheric

* Corresponding author. Fax: +55 91 39456488.

E-mail addresses: cmiranda@usp.br (M.C. Da Cruz Miranda), rossetti@dsr.inpe.br (D. De Fátima Rossetti).

inorganic carbon (O'Leary, 1988). In the marine setting, the isotopic composition of organic matter reflects directly the $\delta^{13}\text{C}$ from C_3 phytoplankton, which is between -20.0% and -22.0% (Hunt, 1970; Newman et al., 1973; Meyers, 1994), because the dissolved bicarbonate used during phytoplankton photosynthesis is 0% .

$\delta^{15}\text{N}$ is applied to differentiate between organic matters derived from aquatic ($\delta^{15}\text{N}$ values around 10.0% or higher) and terrestrial plants (around 0%) (Thornton and McManus, 1994; Meyers, 1997). C/N values above 12 and between 5 and 9 have been related to terrestrial and marine sources, respectively (Bordovskiy, 1965; Prahil et al., 1980; Tyson, 1995; Wilson et al., 2005). Meyers (1994) recorded C/N ratio between 4 and 10 for algae, and around 20 or greater for vascular plants. The mixing of organic matter from different sources may result in $\delta^{13}\text{C}$, $\delta^{15}\text{N}$ and C/N values that fall out of the fields established for terrestrial land plants and phytoplankton (e.g., Lamb et al., 2006), a situation particularly expected in coastal settings.

Several studies have successfully applied $\delta^{13}\text{C}$, $\delta^{15}\text{N}$, and C/N analyses aiming paleoenvironmental reconstructions (e.g., Thornton and McManus, 1994; Ruttenberg and Göni, 1997; Andrews et al., 1998; Müller, 2001; Sifeddine et al., 2001; St-Onge and Hillaire-Marcel, 2001; Westman and Hedenstrom, 2002; Street-Perrott et al., 2004; Wilson et al., 2005). This type of approach can considerably improve the reconstruction of ancient estuarine settings because it helps to recognize deposits formed under marine, fluvial or mixed inflows.

The purpose of the present work was to study late Quaternary deposits from an area in the Amazonian lowland. The analysed core from eastern Marajó Island represents the most complete record of late Quaternary deposits from the Brazilian Amazonia that is available to the scientific community. The continuous nature of the core allows the recognition of several changes in sedimentation pattern through time, providing important data to discuss both the history of relative sea-level fluctuations in northern Brazil and the possible driving mechanisms for these variations.

2. Geological setting

Eastern Marajó Island is located in the Pará Platform (Fig. 1A,B), which corresponds to a broad area of the basement that remained tectonically stable in relation to other sedimentary basins (i.e., Cameté and Limoeiro Sub-basins) of the Marajó Graben System. This structure formed during the opening of the Equatorial South Atlantic Ocean in the Jurassic/early Cretaceous (Sztamari et al., 1987). The Pará Platform is poorly studied, but it might record several small, but deep (up to 3500 m deep), subsiding basins (Azevedo, 1991). The Marajó paleoestuary, which is aligned parallel to the modern Lake Arari, forms a north/southward trend that conforms to a subsurface structure linked to the Mexiana Sub-Basin, an offshore component of the Marajó Graben System (Rossetti et al., 2008b).

The sedimentary fill of the Mexiana Sub-Basin, known only from subsurface data, includes Cretaceous to Quaternary, transitional to fluvial and shallow-marine deposits. Sandy deposits from the Breves/Jacarezinho Formations (Aptian–Cenomanian), and silty–mudstones from the Anajás Formation (Cenomanian) are superimposed by sandstones, mudstones and conglomerates from the Limoeiro Formation (late Cretaceous). These deposits are overlain by a Tertiary succession represented by mixed siliciclastic–carbonate deposits of the Marajó Formation (Paleocene–Eocene), and sandstones (Tucunaré Formation) and mudstones (Pirarucu Formation) of the Pará Group (Miocene to Holocene). In the surface, the Tertiary deposits are recorded by the Pirabas and Barreiras Formations (Miocene), and the post-Barreiras Sediments (Plio–Pleistocene/Holocene).

Northeastern Marajó Island is dominated by Quaternary deposits related to the last depositional phase of the Tucunaré/Pirarucu succession (cf. Vital, 1988). A regional study has included the Marajó Island as part of the Marajoara Structural Compartment, which comprises a set of NW–SE normal faults, segmented by NE–SW and

ENE–WSW/E–W dextral strike–slip faults (Costa and Hasui, 1997; Costa et al., 2001, 2002, Fig. 1A). Recent studies have shown the importance of regional tectonics in the development of many modern drainage and paleodrainage systems in Marajó Island (Rossetti and Valeriano, 2006; Rossetti et al., 2007). Lake Arari is located in an area with several NW–SE and NE–SW tectonic lineaments related to faults (Rossetti et al., 2008b).

3. Materials and methods

Core FSM-1 was obtained 13 km to the west of Lake Arari (Fig. 1B). This area is characterized by elevations averaging 4–6 m above the modern sea-level, and vegetation mostly of grassland savanna, locally known as *campos*. The core was obtained with a LONGYAR 40 rotating drilling system. The recovered core, 124 m long and 60 mm in diameter, provided the basis for facies analysis. Facies descriptions include observations of color, lithology, texture and structure. The sedimentary facies were photographed and recorded on a measured lithostratigraphic profile, which also provided the basis for selecting the samples for laboratory analysis.

Thirteen radiocarbon analyses were undertaken at the Beta Analytic Radiocarbon Dating Laboratory. Organic sediments were dated by scintillation spectrometer and accelerator mass spectrometer (AMS). The samples underwent standard pretreatment (acid–alkaline–acid wash). The conventional ^{14}C ages were corrected to isotopic fractionation. The 2-sigma dates are based on tree-ring data as calibration curves using the Pretoria Calibration Procedure Program (Talma and Vogel, 1993).

A total of 136 sediment samples were collected from core FSM-1 according to changes in sedimentary facies. $\delta^{13}\text{C}$, $\delta^{15}\text{N}$, TOC (total organic carbon) and TN (total nitrogen) analyses were carried out at CENA (Center of Nuclear Energy and Agriculture), Institute of the University of São Paulo-USP, using a Continuous Flow Isotopic Ratio Mass Spectrometer (CF-IRMS). The samples, circa 1 g each, were subdivided for measuring carbon (organic and $\delta^{13}\text{C}$) and nitrogen ($\delta^{15}\text{N}$ and total). The values of $\delta^{13}\text{C}$ and $\delta^{15}\text{N}$ are presented in ‰, relative to the VPDB (Viana Pee Dee Belemite) and atmospheric N_2 , respectively. The TOC and TN provided data for determining C/N values.

4. Facies description

Core FSM-1 contains massive or incipiently-stratified sands and muds interbedded with heterolithic deposits. These include seven sedimentary facies (Table 1): massive sand (facies Sm), parallel laminated sand (facies Sp), cross laminated sand (facies Sc), massive pelite (Pm), parallel mud and streaky heterolithic bedded deposits (facies Mp/Hs), lenticular (facies Hl) and wavy/flaser (facies Hwf) heterolithic bedded deposits. The massive nature of facies Sm might result, in part, from destruction of original structures during drilling. Most of the facies are interbedded with deposits displaying ductile and brittle soft sediment deformation (i.e., convolute fold, ball-and-pillow, pygmatic fold, oversteepened undulation, microfracture and fault) structures. These features were related to syn-sedimentary seismicity in a previous publication (Rossetti et al., 2007), which should be consulted for further details. The sedimentary facies were organized into six associations (Table 2), described below, and attributed to different depositional environments of an estuarine system (Figs. 2A–B and 3).

4.1. Facies association A: fluvial channel

This association reaches up to 47 m thick, being recorded in two depth intervals, one between 93 and 124 m, and the other between 68 and 77 m. It consists mostly of moderately sorted, fine to coarse-grained, locally conglomeratic, massive sand (facies Sm), with

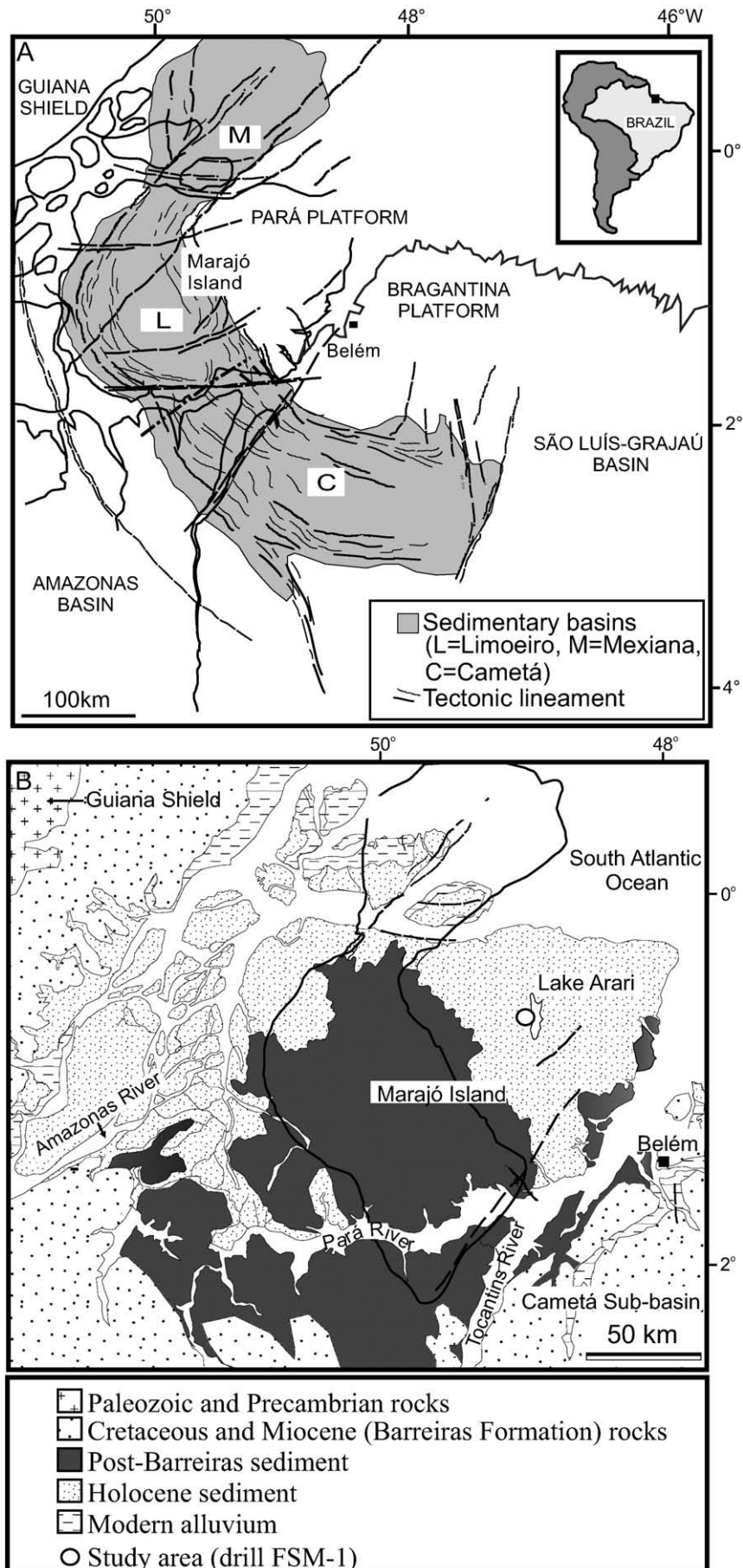


Fig. 1. A) Regional geology of the study area in the Limoeiro Basin of the Marajó Graben System, northern Brazil, showing the location of the main tectonic lineaments. B) Detailed map showing the location of the study area in the eastern margin of Lake Arari, with the distribution of the geological units.

Table 1
Lithofacies descriptions of core FSM-1, from the western margin of Lake Arari, eastern Marajó Island.

Facies	Description	Sedimentary process
Massive sand (Sm)	Light yellow, moderately sorted, fine-grained massive sand. Mud intraclasts are either disperse or locally form conglomeratic lags up to 0.2 m thick.	The massive nature of these deposits might have been produced during drilling. Therefore, the most likely is that these deposits were, at least in great part, stratified.
Parallel-laminated sand (Sp)	Fine-to-medium grained sand with parallel lamination or stratification. Local association with mud drapes. Undetermined trace fossils are locally found.	High (upper plane bed) energy flows. Parallel laminated sands with mud interbedding are related to low energy flows, before the stage of ripple development.
Cross laminated sand (Sc)	Dark yellow, well sorted, fine- to medium-grained sand with current and wave ripple cross lamination	Migration of small ripples formed during low energy, either unidirectional or combined (unidirectional and oscillatory) flows.
Massive pelite (Pm)	Gray, endured and massive pelite. Local reddish and/or yellow mottling, as well as root marks.	Sediment homogenization by biologic activity and/or pedogenetic processes.
Parallel laminated mud and streaky heterolithic bedded deposit (Mp/Hs)	Plastic, gray to black mud with parallel lamination and muds with thin, continuous streaks of gray to olive, silty to very fine-grained sand.	Deposition of mud from suspension under very low flow energy. The heterolithic deposits record also low energy flows, but with episodic sand input during relatively higher flow energy.
Lenticular heterolithic heterolithic bedded deposit (Hl)	Gray to black mud with discontinuous lenses of gray to olive, silty, very fine- to fine-grained sand. The sand lenses might display cross lamination.	Low flow energy, with mud deposition from suspension, but with periodic sand inflows, mostly trough migration of starving ripples.
Wavy and flaser heterolithic deposits (Hwf)	Gray to black mud layers interbedded with fine- to medium-grained sand forming wavy and flaser structures.	Fluctuating low and relatively higher flow energies, with a balance between mud deposition from suspensions and sand deposition either from suspension or migrating ripples.

subordinate parallel laminated mud (facies Mp). These lithotypes are typically arranged into several fining upward cycles that vary in thickness from 0.1 m to 8 m. The base of these cycles, sharp and usually erosive, is locally marked by mud intraclasts. These, as well as quartz granules and plant debris, are also dispersed within the sands. Deposits in facies association A have a distinctive isotopic signature: $\delta^{13}\text{C}$ -17.37% to -27.21% (mean = -22.64%), $\delta^{15}\text{N}$ -6.85% to $+11.67\%$ (mean = $+3.66\%$), and C/N 12.45 to 43.26 (mean = 24.77). Noteworthy is the $\delta^{13}\text{C}$ values that become slightly depleted in the upper half of this facies association, and the inverse correlation between $\delta^{13}\text{C}$ and the C/N values.

4.2. Facies association B: outer estuarine basin to shallow marine

This facies association (Fig. 2B) is observed between the depth interval of 44 and 64 m, where it overlies facies association C. Facies association B is sharp bounded and dominantly muddy, consisting mostly of parallel mud and streaky heterolithic bedded deposits (facies Mp/Hs). These strata are interbedded with numerous packages of lenticular and wavy to flaser heterolithic deposits, corresponding to facies Hl and Hwf, respectively. The sandier heterolithic packages vary from 0.2 m to 2 m thick and grade upward from facies Mp/Hs to form

coarsening upward successions. Thicker sand layers locally display combined flow cross lamination. Plant debris is dispersed throughout this facies association, as are mud intraclasts. The $\delta^{13}\text{C}$ values are more variable with respect to the previous facies association, ranging from $\delta^{13}\text{C}$ -16.65% to -23.38% , with a heavier mean of -21.63% . In contrast, the $\delta^{15}\text{N}$ values are less variable than in facies association A, ranging from $+3.83\%$ to $+9.43\%$, with a higher mean of $+6.75\%$. C/N values vary from 5.3 to 11.54, with a mean of 7.05.

4.3. Facies association C: inner estuarine basin

This facies association (Fig. 2B) occurs between the depth intervals of 64–68 m and 77–93 m. The deposits are lithologically similar to association B, being characterized by parallel mud and streaky heterolithic bedded deposits (facies Mp/Hs). They are also organized into numerous coarsening upward cycles up to 2.0 m thick and formed by lenticular (facies Hl) and wavy to flaser heterolithic (facies Hwf) deposits. More rarely, fining upward successions are also present. Despite the similarity to facies association B, this association was distinguished isotopically by less negative $\delta^{13}\text{C}$ values between -10.35% and -26.78% (mean = -18.46%), $\delta^{15}\text{N}$ values between $+3.77\%$ and $+9.35\%$ (mean = 6.17%), and C/N between 14.74 and 26.81 (mean = 18.44).

4.4. Facies association D: tidal flat

This association (Fig. 2A) corresponds to a short interval between 33 and 44 m depth, which grades downward into facies association B (Fig. 3). This unit consists mostly of lenticular and wavy to flaser heterolithic deposits (facies Hl and Hwf), locally interbedded with packages of massive sands (facies Sm) up to 1 m thick. The strata are typically intergraded, forming sharp-based, fining upward cycles up to 4 m thick. Plant debris are locally present in this facies association. Despite the increased sand content relative to facies association B, these deposits display comparable $\delta^{13}\text{C}$ and $\delta^{15}\text{N}$ values, which vary from -18.57% to -25.85% (mean = -21.53%) and $+3.81\%$ to $+12.14\%$ (mean = $+8.17$), respectively. C/N values are generally higher, ranging from 6.96 to 21.66 (mean = 13.54).

4.5. Facies association E: estuarine channel

This association (Fig. 2A), which occurs between 18 and 33 m depth, consists of a sharp-based, medium- to coarse-grained sandy package that grades upward into facies association F, described below (Fig. 3). The interval is nearly 15 m thick and comprises several, also sharp-based, fining and thinning upward cycles. This facies association is represented by massive sand (facies Sm), cross laminated sand (facies Sc) and, subordinately, lenticular heterolithic bedded deposit (facies Hl), as well as wavy and flaser heterolithic bedded deposits (facies Hwf). The cross laminated sets in facies Sc display *foresets* frequently covered by mud films. Mud intraclasts and wood fragments are abundant, and undetermined trace fossils are locally present. $\delta^{13}\text{C}$ values range from -20.78% to -25.00% (mean = -22.24%). The $\delta^{15}\text{N}$ and the C/N values range from -4.73% to $+13.13\%$ (mean = $+3.35\%$) and 8.80 to 30.00 (mean = 22.23), respectively. The isotopic values are more variable in the lower portion of this facies association, while upward they become noticeably more constant, with a sharp contrast in the values at 18 m depth.

4.6. Facies association F: lagoon

As with facies association B, this association is dominantly represented by muddy and heterolithic deposits, occurring above approximately 18 m depth. This interval consists mostly of parallel mud and streaky heterolithic bedded deposits (facies Mp/Hs). In addition, the strata are also interbedded with numerous coarsening

Table 2

Description of facies associations with corresponding interpretation of the organic matter sources and paleoenvironments.

Facies association	Interpreted paleoenvironment	Description	Main source of organic matter (interpreted from $\delta^{13}\text{C}$, $\delta^{15}\text{N}$ and C/N)
A	Fluvial channel	Moderately sorted, fine to coarse-grained, locally conglomeratic, massive sand (facies Sm), with only subordinate parallel laminated mud (facies Mp). These lithotypes are typically arranged into several fining upward cycles, which vary in thickness from 0.1 m to 8 m. The base of these cycles, sharp and usually erosive, is locally marked by mud intraclasts. A few mud intraclasts, as well as quartz granules, are dispersed within the sands, as are plant debris	Terrigenous origin, with organic carbon derived mainly from C ₃ vascular vegetation
B	Outer estuarine basin to shallow marine	Dominantly muddy, consisting mostly of parallel mud and streaky heterolithic bedded deposits (facies Mp/Hs). Interbedded with numerous packages of lenticular and wavy to flaser heterolithic deposits, corresponding to facies Hl and Hwf, respectively. The sandier heterolithic packages vary from 0.2 m to 2 m thick, and grade upward from facies Mp/Hs, forming coarsening upward successions. Thicker sand layers locally display combined flow cross lamination. Plant debris are dispersed throughout this facies association, as are mud intraclasts.	Terrestrial (both C ₃ and C ₄ plants), phytoplankton (marine and freshwater), and mixed organic matter sources
C	Inner estuarine basin	Facies characteristics as unit 1b, though thinner (up to 10 m thick). Coarsening and fining upward cycles.	Freshwater phytoplankton, as well as C ₃ and C ₄ vascular vegetation
D	Tidal flat	Lenticular and wavy to flaser heterolithic deposits (facies Hl and Hw/f), which are locally interbedded with packages of massive sands (facies Sm) up to 1 m thick. These strata are typically intergraded, forming sharp-based, fining upward cycles up to 4 m thick. Plant debris are locally present in this facies association	Marine or freshwater phytoplankton source, or even a mixture of both. Contributions of C ₃ and C ₄ land plants are also recorded
E	Estuarine channel	Sharp-based unit up to 15 m thick, consisting of coarse- to fine-grained sand and, secondarily, heterolithic deposits arranged into fining and thinning upward cycles. Reactivation surfaces, mud drapes and mud clasts are abundant	C ₃ terrestrial plants, but with episodes of either marine phytoplankton or mixed marine and land plant inputs
F	Lagoon	An 18 m-thick unit located at the top of the studied section. Sandier at the base and muddier upward, and arranged into fining and coarsening upward cycles. Muddier cycles prevail upward in the section. Dispersed plant debris	Strong marine influence, except for a few intervals, where mixed marine and terrigenous sources are evident, particularly in the uppermost portion of the succession



Fig. 2. Examples of cores from drill FSM-1 from two intervals; A) Depth interval 29.60–35.00 m, where estuarine channel sands overlie tidal flat muds and heterolithic deposits. Note the sharp boundary between these depositional settings, which is related to a sequence boundary (SB) and a transgressive surface (TS); B) Depth interval 57.60–65.00 m, where inner estuarine basin deposits are overlain by outer estuarine basin interbedded sands, muds and heterolithic deposits, with a transgressive surface (TS) indicated at depth 61.80 m.

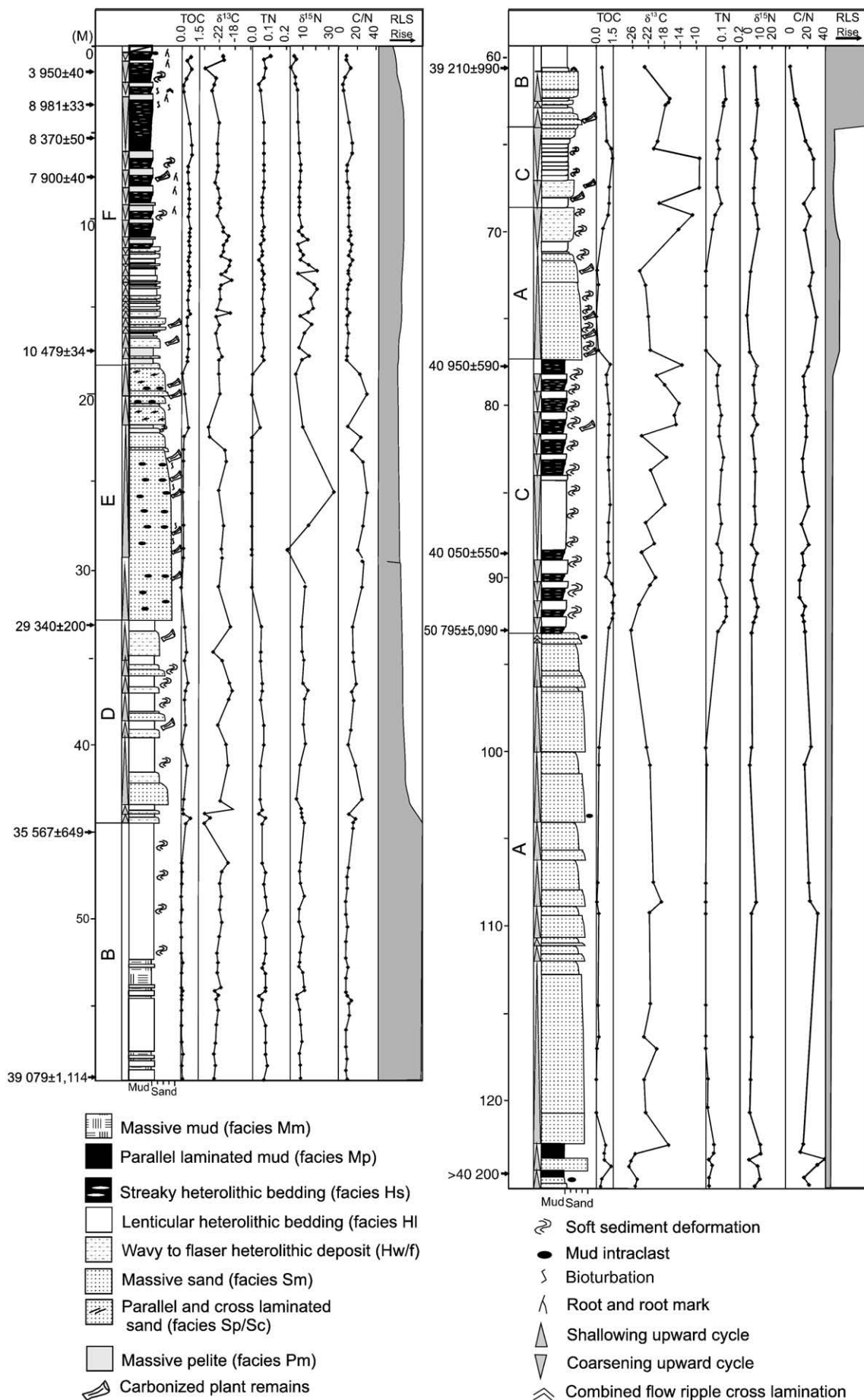


Table 3

Radiocarbon ages of core FSM-1. All ages derive from AMS analysis of organic matter derived from organic mud.

Sample	# Depth (m)	Type of material	Conventional ^{14}C yr B.P.	2-sigma calibration (Cal B.P.)
SM-1-72	1.3	Organic sediment	3940 ± 40	4510–4470; 4450–4250
SM-1	3.0		8981 ± 33 ^a	10,114–10,239
SM-78	5.6		8370 ± 55 ^a	9490–9280
SM-10	7.5		7900 ± 40	8980–8820; 8800–8600
SM-24	17.5		10,489 ± 34	12,364–12,674
SM1-134	33		29,340 ± 200	–
SM-36	45		35,567 ± 649	–
SM-60	57		39,079 ± 1114	–
SM-1-172	61		39,210 ± 990	–
SM-1-189	77		40,950 ± 590	–
SM-1-198	89		40,050 ± 550 ^b	–
SM-1-206	93.20		50,795 ± 5090	–
SM-1-214	124		>40,200	–

– Samples not suitable for calibration.

^a Age disregarded in this analysis due to possible reworking of organic matter.

^b Age disregarded in this analysis due to possible carbon rejuvenation.

upward and, more rarely, fining upward cycles up to 3 m thick comprising lenticular and wavy to flaser heterolithic deposits (facies H1 and Hwf). Plant debris and root marks are dispersed within this uppermost interval of the analysed core. The $\delta^{13}\text{C}$ values have a uniform distribution along this association relative to other associations described, ranging from -18.15‰ to -25.76‰ (mean = -21.71‰). The $\delta^{15}\text{N}$ and the C/N values range from $+1.06\text{‰}$ to $+27.34\text{‰}$ (mean = $+10.34\text{‰}$) and 2.45 to 13.31 (mean = 8.78), respectively. Note that the isotope and the C/N values decrease slightly towards the upper boundary of this unit.

5. Core chronology

The AMS analysis of Lake Arari core provided ages ranging from 3950 (± 40) ^{14}C yr B.P. to 50,795 (± 5090) ^{14}C yr B.P. (Table 3), which suggest deposition during the Late Pleistocene to early/middle Holocene. The youngest dating derives from sediments located around 1.3 m depth, thus deposition of the upper part of the profile might be even younger. The latter age is close to the limit of radiocarbon dating. Consequently, it might include deposits that are considerably older than the indicated value, though AMS analysis allows ages up to 57,000 yr B.P. to be suggested. The more basal sample (SM214) was not considered in this analysis, because it indicates an undetermined age beyond 40,200 ^{14}C yr B.P. In addition, local age inversion was detected in the uppermost interval. Hence, samples SM1 and SM78 are only slightly older than expected considering their stratigraphic position and the ages obtained below (SM10) and above (SM72). Samples SM1 and SM78 might contain reworked organic matter, but the small age difference between these samples relative to the two underlying ones suggests that this organic matter was derived from immediately underlying deposits. Additionally, there is an age conflict comparing the samples SM189 and SM198, with the latter being unexpectedly slightly younger than the first despite its stratigraphically lower position. One possibility is that sample SM189 also might contain organic matter derived from reworking of immediately underlying strata. However, it is most likely that the age indicated by sample SM198 results from carbon rejuvenation, as suggested by the analysis of sedimentation rate provided below. Therefore, disregarding samples SM1 and SM78, and perhaps SM198, the ages are, in general, progressively older downward through the core, attesting to general dating consistency. Even taking into account the samples with age inversions, local reworking of organic matter is suggested by the small difference in age compared with the immediately underlying strata.

Consequently, a Late Pleistocene to early/middle Holocene is confirmed for the bulk of the studied section.

If one considers constant sediment deposition, the age of 50,795 \pm 5090 ^{14}C yr B.P. recorded at depth 93 m would provide an overall estimated sedimentation rate of 1.8 mm/yr. However, when specific intervals with defined ages are analysed, estimated sedimentation rates might be variable. For example, the uppermost 60 m interval records a sedimentation rate of 1.8 mm/yr, while a higher sedimentation rate is recorded for the lower half of the profile. Hence, considering the ages depicted in Table 3 and Fig. 3, a sedimentation rate of 3.5 mm/yr is indicated between 62 and 88 m. In contrast, the lowest sedimentation rate of only 0.5 mm/yr is recorded in the immediately underlying interval between 88 m and 93 m. If one takes into account that these two intervals display deposits formed continuously by similar sedimentary processes, then most likely the age indicated for sample SM 1–198 is not correct, as discussed above, possibly resulting from contamination by younger carbon during sample handling. Excluding this age (i.e., 40,050 \pm 556 yr B.P.), the interval 62–93 m would provide a sedimentation rate of 2.8 mm/yr.

6. Palaeoenvironmental interpretation

Previous work, based mostly on remote sensing, revealed an exceptionally well preserved palimpsest funnel-shaped morphology in the area of Lake Arari, which was interpreted as a broad Late Pleistocene to Holocene estuary (Rossetti and Valeriano, 2006; Rossetti et al., 2007). These authors have also proposed that the abandonment of this estuary occurred when fluvial inflows, derived from continental areas, were interrupted. This process is related to the eastern detachment of Marajó Island from the mainland due to reactivation of tectonic faults (Rossetti et al., 2007).

The studied core is located only 13 km to the west of Lake Arari, thus it should contain some deposits from this palaeoestuarine system. Indeed, integration of ^{14}C dating, facies analysis and isotope data revealed that the 120 m long core contains Late Pleistocene and Holocene deposits varying from fluvial to estuarine, lagoonal and finally lacustrine environments.

Application of $\delta^{13}\text{C}$, $\delta^{15}\text{N}$, and C/N analyses have helped to distinguish marine, non-marine and mixed influenced deposits, leading to the better understanding of the depositional system. The use of these proxies as palaeoenvironmental indicators might be debatable, considering several possible influences, mostly grain size, diagenesis and CO_2 variation through time.

Larger sediment grain sizes have higher potential to transport bigger particles of terrestrial plants, which might provide higher C/N values, though there is no influence on the carbon and nitrogen isotopic compositions (e.g., Thompson and Eglinton, 1978; Keil et al., 1994; Prahl et al., 1994). In contrast, fine-grained sediments have higher volumes of clay minerals, which adsorb ammonia, contributing to a decrease in the C/N value due to the uptake of inorganic nitrogen (Meyers, 1997). In the study area, the changes in $\delta^{13}\text{C}$, $\delta^{15}\text{N}$, and C/N do not systematically follow grain size variation. For instance, thick sediment packages with comparable grain sizes related to facies associations representative of different depositional settings display contrasting sets of carbon and nitrogen isotope values and C/N ratios (for instance, compare intervals 44–60 m, 77–93 m, and the uppermost 18 m of the profile, which consist of similar sand and mud interbeddings) (Fig. 3). Thus, the distribution of $\delta^{13}\text{C}$, $\delta^{15}\text{N}$, and C/N in the studied profile appears to have been controlled by differences in organic matter sourced into the depositional settings, rather than grain size.

Another potentially influencing factor is the biodegradation of organic matter that might start rapidly even in the water column due to the action of aerobic microbes, which causes modification of the $\delta^{13}\text{C}$, $\delta^{15}\text{N}$ and C/N signals (e.g., Thornton and McManus, 1994; Middelburg and

Fig. 3. Lithostratigraphic profile of core FSM-1 showing the facies assemblages and the corresponding TOC, TN, $\delta^{13}\text{C}$, $\delta^{15}\text{N}$ and C/N values. (A = fluvial dominated channel; B = outer estuarine basin to shallow marine; C = inner estuarine basin; D = tidal flat; E = estuarine channel; F = lagoon; RLS = relative sea level).

Nieuwenhuize, 1998; Cloern et al., 2002, see also several references in Lamb et al., 2006 and Chen et al., 2008). The decomposition of organic matter along the water column decreases the $\delta^{13}\text{C}$, reflecting different $\delta^{13}\text{C}$ values of labile and refractory organic material. However, there is an overall agreement among these authors that this value remains relatively constant in the sediment, due to the presence of ^{13}C -rich organisms in the biomass. Likewise, the C/N seems to remain fairly constant after burial. Therefore, these proxies can be used as reliable indicators of Quaternary paleoenvironments. On the other hand, the degradation of organic matter might cause either a depletion or enrichment of ^{15}N (e.g., Saino and Hattori, 1980; Fry et al., 1991; Nakatsuka et al., 1997; Sachs and Repeta, 1999; Lehmann et al., 2002) due to the biosynthesis of inorganic nitrogen (e.g., Meyers, 1997; Chen et al., 2008). As a result, $\delta^{15}\text{N}$ should not be used solely for paleoenvironmental reconstruction, though it might be combined with other proxies to improve the interpretation.

The increase in atmospheric CO_2 by approximately 20% since the last glacial maximum (LGM) (Adams et al., 1990; Behling 2002) might also have influenced the $\delta^{13}\text{C}$ values of the studied late Quaternary deposits, affecting the proposed paleoenvironmental interpretation. However, a study considering a large range of atmospheric carbon dioxide concentrations showed no systematic variation in the $\delta^{13}\text{C}$ value of plant tissues (Arens et al., 2000). In addition, a decrease of only about 0.3‰ in the carbon isotope of surface water and 0.35‰ in terrestrial organic carbon transferred to the ocean-atmospheric reservoir has been documented since the LGM (Hofmann et al., 1999). Taking these studies into account, it is assumed that the changes in atmospheric CO_2 through time did not affect significantly the $\delta^{13}\text{C}$ values reported herein.

In general, there is a good correspondence of $\delta^{13}\text{C}$, $\delta^{15}\text{N}$ and C/N values with individual facies associations, which is interpreted to reflect the primary signature of the organic matter preserved in the analysed sediments. Moreover, the isotopic and geochemical values of facies associations are typical of those recorded in late Quaternary deposits from other estuarine systems (e.g., Salomons and Mook, 1981; Peterson and Howarth, 1987; Middelburg and Nieuwenhuize, 1998; Wilson et al., 2005).

Facies association A is attributed to fluvial channels. Although a channel geometry could not be spatially determined because only one core has been retrieved and analysed, a channel interpretation is consistent with the several sharp-based and fining upward cycles, as well as the prevalence of conglomeratic and coarse- to medium-grained sands. These features indicate high energy, with alternating periods of erosion and deposition, and decreasing flow energy through time, conforming to channel fills (Allen, 1982; Atchley et al., 2004; McLaurin and Steel, 2007). The prevalence of more negative $\delta^{13}\text{C}$ values, together with high and low values of C/N and $\delta^{15}\text{N}$, respectively, suggests that the organic matter preserved in these sediments is of terrestrial origin, with organic carbon derived mainly from C_3 vascular vegetation. This organic matter source is characteristic of fluvial channels. However, a few samples display $\delta^{15}\text{N}$ values within the range of aquatic plants (Thornton and McManus, 1994; Meyers, 1997; Cloern et al., 2002), and the binary plots of $\delta^{13}\text{C}$ versus C/N (Fig. 4A) revealed a contribution from mixed C_3 land plants and marine phytoplankton sources. Therefore, it is concluded that the fluvial system was located near to a coastal setting, being eventually affected by the introduction of organic matter derived from the marine realm due to the influence of waves and tidal currents. The overall absence of muds in the fining upward cycles indicates that floodplains were probably not present. If present, the floodplains were poorly developed, forming thin deposits that were more likely to be completely reworked during channel dynamics, a process suggested by the frequent mud intraclasts. Thus, facies characteristics suggest either braided fluvial systems (Van de Graaff, 1972; Nichols and Fisher, 2007) or long term amalgamation of highly sinuous sandy channel belts, where the record of floodplains was destroyed during channel migration.

Facies association B records low energy subaqueous environments, indicated by the abundance of parallel muds derived from suspensions. The thick nature (i.e., up to 27 m thick) suggests a relatively

large standing water body which, in this environmental context, could be related to an estuarine basin setting. This part of an estuary is characterized by a turbulence zone, where a high volume of mud is kept in suspension due to the interaction of fluvial and marine inflows (Dalrymple et al., 1992). An estuarine basin is further supported by the overall $\delta^{13}\text{C}$, $\delta^{15}\text{N}$, and C/N values, which indicate dominance of marine phytoplankton (Fig. 4B). The muddy nature, and the fairly constant $\delta^{13}\text{C}$ values with a negative mean (-21.63%), as well as the low C/N mean (7.05), indicate strong marine influence suggestive of deposition either in the outer estuarine basin, or in fully shallow-marine environments out of the estuarine system.

The muddy nature of association C indicates a low energy depositional setting. Stable isotope and C/N values suggest that the organic source was dominantly freshwater phytoplankton, as well as C_3 and C_4 plants, with a minor contribution from mixed marine and freshwater sources. Considering the proposed depositional context, these characteristics conform to sedimentation in the inner estuarine basin (Fig. 4B), where fluvial inflows were frequent. The coarsening upward cycles attest to episodic introduction of sands into the low energy basin, which is related to prograding suspension lobes. The occurrence of facies association C above fluvial channel deposits (association A) suggests that these lobes are more likely bayhead deltas. This interpretation is consistent with the fact that the coarsening upward cycles display a higher abundance of organic matter derived from C_3 and C_4 vascular plants relatively to the rest of this facies association.

Facies association D records several episodes of sand and mud deposition under decreasing energy flow, as indicated by the sharp-based fining upward cycles. This association displays organic carbon derived either from marine or freshwater phytoplankton, or even a mixture of both (Fig. 4C). Contributions of C_3 and C_4 land plants are also recorded in this association. The physical and chemical characteristics of this unit, together with its stratigraphic location overlying estuarine central basin deposits and underlying estuarine channel deposits, indicate a possible tidal flat setting. Therefore, the fining upward cycles might record deposition of sands and muds in the transition from subtidal to intertidal zones, as recorded in many other tidal settings (e.g. Martino, 1996; Fenies and Faugères, 1998).

Facies association E is related to an estuarine channel environment. Channel characteristics are revealed by the sharp and, erosive base, the abundance of mud intraclasts indicative of sediment reworking under high energy flows, and the several fining and thinning upward cycles recording a successive decrease in flow energy through time. Although tidal bundles could not be recognized, deposition by tidal currents is locally suggested by frequent mud drapes along the foresets (e.g. Frey and Howard, 1986; Martino, 1996). Bioturbation is expected in this setting (e.g., Frey and Pemberton, 1984; Martino and Sanderson, 1993), which was recorded in abundance in this facies association. An estuarine nature is further supported by $\delta^{13}\text{C}$, $\delta^{15}\text{N}$ and C/N values, which indicate mixed marine and fluvial-derived organic matter sources. This is revealed by sediments with organic carbon derived dominantly from C_3 terrestrial plants, but with episodes of either marine phytoplankton or mixed marine and land plant inputs (Fig. 4D). Moreover, these deposits record alternating marine and fluvial inflows, with the latter prevailing. This is indicated by the overall higher C/N values suggesting a significant input of terrigenous organic material, as documented in many estuarine channel environments (Thornton and McManus, 1994; Ruttenberg and Göni, 1997; Sifeddine et al., 2001; St-Onge and Hillaire-Marcel, 2001; Westman and Hedenstrom, 2002; Street-Perrott et al., 2004; Wilson et al., 2005). Therefore, this facies association is related to an estuarine channel with strong fluvial influence. Indeed, the stratigraphic location between tidal flat and lagoonal deposits (facies association F, discussed below) is consistent with an estuarine channel interpretation.

Facies association F records mud deposition from suspensions within a dominantly low energy depositional environment. The isotope and C/N data indicate a strong marine influence, except for a few intervals, where mixed marine and terrigenous sources are evident, particularly in

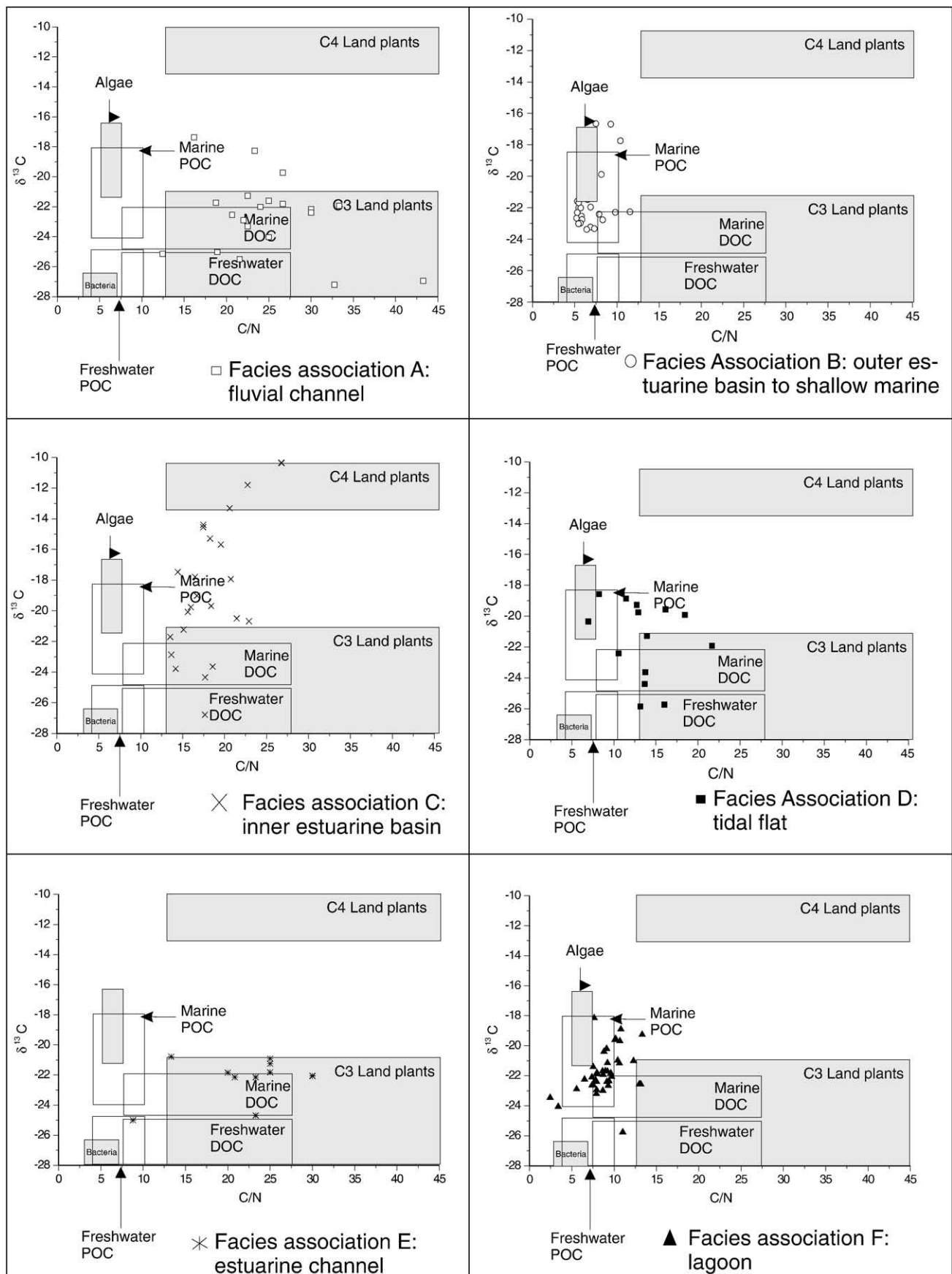


Fig. 4. A–F) Binary diagrams of $\delta^{13}\text{C}$ and C/N for individual depositional environments recognized in the study area, with interpretation of sources of the organic matter based on typical ranges recorded in several coastal environments (compiled from Bordovskiy, 1965; Haines, 1976; Deines, 1980; Sherr, 1982; Schidlowski et al., 1983; Meyers, 1994; Peterson et al., 1994; Schleser, 1995; Tyson, 1995; Middelburg and Nieuwenhuize, 1998; Chivas et al., 2001; Raymond and Bauer, 2001; Cloern et al., 2002; Goñi et al., 2003; and references therein).

the uppermost portion of the succession (Fig. 4E). The presence of root marks indicates an environment with frequent subaerial exposure. Taken together, the deposits indicate either a lagoon or estuarine basin environment, although a lagoonal environment is more likely due to the overall prevalence of marine conditions throughout. The slight upward increase in the isotope and C/N values favours a slight reduction in marine influence over time, though these values do not support a permanent connection to a fluvial inflow. The numerous coarsening upward cycles suggest that deposits displaying this lithological pattern are also present in facies association B, where they were related to bayhead deltas. Taking into account the marine nature of this setting, the coarsening upward deposits could record either tidal deltas or successive episodes of lagoon shallowing.

7. Relative sea-level dynamics

Analysis of the stratal architecture of the Late Pleistocene and Holocene deposits reveals that sedimentation took place mostly under estuarine conditions. The estuary did not evolve continuously, but was interrupted by several episodes of transgression and regression, as indicated by the cyclical nature of the deposits (Fig. 5A–H). There is an overall prevalence of fluvial conditions from the base of the profile up to a depth of 61 m, while the sediments above this depth record a greater marine influence. Deposition started within terminal amalgamated fluvial channels, rarely affected by marine inflows (Fig. 5A). The overlain deposits are related to an inner estuarine basin, represented by the interval depth of 77–93 m, which records the period between 40,950 (± 590) and 50,795 ^{14}C yr B.P. The vertical superposition of fluvial deposits by inner estuarine basin deposits requires a rise in relative sea level (Fig. 5B). The fluvial channel deposits between depths 71–77 m suggest a renewed episode of fluvial incision and progradation over the inner estuarine basin, which could be related to a drop in relative sea level (Fig. 5B) or a punctuated phase of low relative sea level. This lowering, recorded between 39,079 (± 1114) and 40,950 (± 590) ^{14}C yr B.P., was followed by migration of inner estuarine basin over fluvial deposits (facies association C; Fig. 5C).

Following regression, there was a period of significant relative sea-level rise (Fig. 5D), as recorded in the interval depth of 64–44 m. These deposits are dominantly muddy and contain organic carbon derived mostly from marine phytoplankton, which supports deposition in the outer estuarine basin to open shallow-marine settings. The superposition of these deposits directly on inner estuarine basin deposits indicates a significant transgression between 35,507 (± 645) and 39,079 (± 1114) ^{14}C yr B.P.

The tidal flat deposits (facies association D) between depths 33 and 44 m suggest a period of relative sea-level stability or fall after the previous transgression (Fig. 5E). As this tendency for relative sea-level fall became more pronounced, subaerial exposure and stream scouring took place (Fig. 5F), followed by fluvial rejuvenation and establishment of an estuarine valley after 29,340 (± 340) ^{14}C yr B.P. (Fig. 5G). Overlying the basal unconformity recorded at 33 m depth, sediment was deposited within the valley, forming an overall fining upward succession as a result of a progressive decrease in flow energy through time up to the core surface. The lower portion of this succession (18–33 m depth) is due to high flow energy in estuarine channel settings having strong fluvial influence (facies association E). The fluvial inflow was interrupted around 10,479 (± 34) ^{14}C yr B.P., as a result of the estuary evolution into a lagoon (Fig. 5H). During this time, the organic sediment inflow into the study area was derived mostly from the north, i.e., from the sea. A relative sea-level fall was in effect in the latest Holocene, which resulted in northward coastal progradation, a process that would have culminated with the evolution of the lagoon into the Lake Arari. The presence of sediments with marine derived organic matter near the top (approximately 3 m from surface) of the core reveals that the establishment of this lake took place very recently.

8. Tectono-sedimentary evolution

Estuaries represent important components of incised valley systems (Zaitlin and Shultz, 1990; Dalrymple et al., 1992; Zaitlin et al., 1994; Dalrymple, 2006). Analysis of estuarine incised valley deposits allows an insight into coastal sediment dynamics and sea-level change. Many studies have related the origin and evolution of incised valleys to eustatic changes (see several papers in Dalrymple et al., 1994). However, an increasing number of studies have related the origin and evolution of incised valleys to climate changes or tectonic activity (Zaitlin et al., 2002, see also several paper in Dalrymple et al., 2006). Differentiating between eustasy, tectonics and climate, is still a challenge for the stratigraphers and sedimentologists. The reconstructed relative sea-level history of Marajó Island can be combined with available geological data to determine the possible driving mechanisms involved in the evolution of the northern Brazilian coast during the late Quaternary.

Rossetti et al. (2008a) attempted to explain relative sea-level fluctuations in Northern Brazil in the context of regional tectonics. However, their reconstruction was limited to the last 8000 year history of Marajó Island. The present study provides a longer record of late Quaternary environmental change in this area, allowing a discussion, for the first time, of both the history of relative sea-level fluctuations and the possible driving mechanisms over the last 50,000 yr B.P.

The sedimentation rate is distinctively higher (i.e., 2.8 mm/yr) below 60 m depth relative to the uppermost 60 m deposits, which averages 1.8 mm/yr. The high sedimentation rate estimated for the lower half of the profile approaches those recorded from areas with tectonic subsidence (e.g., Nilsen and McLaughlin, 1985). This suggests that tectonic activity may have generated accommodation space during the late Quaternary in Marajó Island. Previous studies have demonstrated that this area has been affected by episodes of fault reactivation even during the Holocene (Costa and Hasui 1997; Rossetti and Valeriano, 2006; Rossetti et al., 2007). Additionally, our ongoing analyses of shallow cores around the study area have revealed great variations in bed thicknesses. Therefore, deposits of Late Pleistocene ages, located at the base (124 m) of core FSM-1, are recorded much higher (i.e., a few meters below the present surface) in some areas indicating that fault displacements were concomitant with sediment accumulation. Moreover, as mentioned by Rossetti et al. (2008b), Marajó Island is in a modern seismic zone where earthquakes with magnitude of up to 4.8 have been recorded (Miotto, 1993).

The prevalence of fluvial dominated deposits recorded between 40,950 (± 590) and 50,795 ^{14}C yr B.P. (Fig. 5B) corresponds to a period of global sea-level lowering related to the expansion of polar ice sheets (e.g. Crowley and North, 1991). However, the transgressive event recorded between 44–64 m (35,507 (± 645) and 39,079 (± 1114) ^{14}C yr B.P.) could be a reflex of regional tectonic subsidence. During this time, the polar ice sheets continued to expand, leading to a worldwide fall in relative sea level. Thus, while eustatic sea level was falling, Marajó Island was undergoing a major transgression that resulted in the replacement of inner estuarine basin muds by outer estuarine basin to shallow-marine muds (facies association B) overlying deposits formed in the inner estuarine basin (facies association C; Fig. 5D). The tidal flat (facies association D) deposits that overlie the transgressive strata could be related to a period of relative sea-level stability (Fig. 5A,C). The inner estuarine basin deposits between 64 and 71 m point to a standing water body dominated by freshwater input near the coastline.

The last depositional episode after 29,340 (± 340) ^{14}C yr B.P., records the stratigraphic nature of the paleoestuary whose morphology is still preserved in the Marajó landscape. Several arguments in support of a tectonic origin for this paleoestuary have already been presented elsewhere (Rossetti et al., 2008b). These authors have also shown that the paleochannels linked to the inner estuarine morphology disappeared suddenly in the eastern margin of Marajó Island. Based on this evidence, they have suggested that eastern Marajó Bay was fluvially influenced

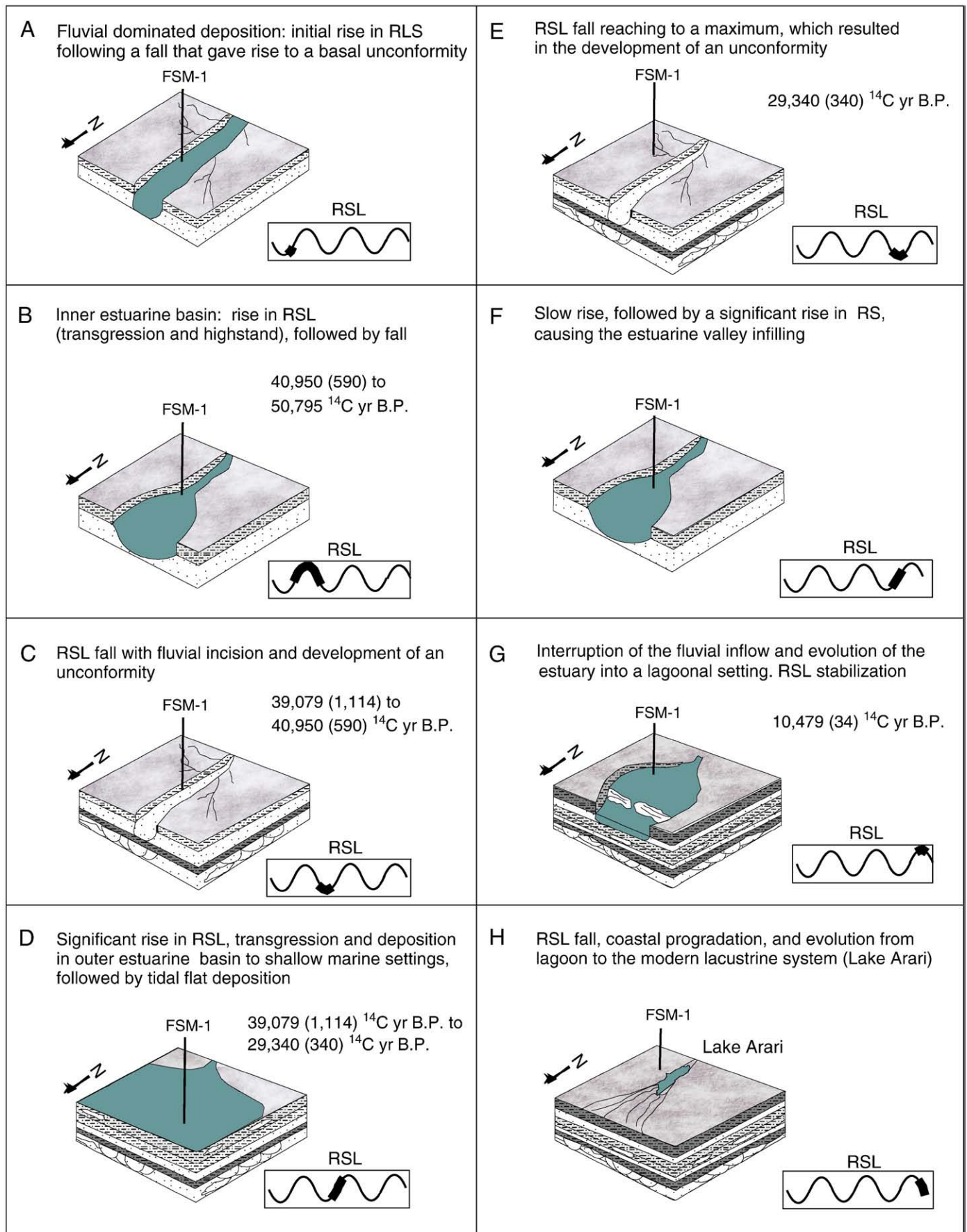


Fig. 5. A–H) Diagrams with the schematic representation of successive phases of sediment accumulation and non-deposition during the Quaternary in the study area within the context of relative sea-level fluctuations (RSL = relative sea-level). See text for further explanations.

prior to the Island detachment as a result of NE–SW trending faults. First, fluvial rejuvenation and incision took place, scouring the paleovalley, which was followed by estuarine deposition. The time range of these events corresponds to two significant glacial events, i.e., the LGM, between 23,000 and 18,000 yr B.P. and the Younger Dryas, between 11,800 and 12,600 yr B.P. (Crowley and North, 1991). One possible interpretation is that the drop in sea level related to these two cold episodes gave rise to the unconformity at the base of the estuarine valley (i.e., 34 m depth), and only then deposition started to fill up the valley. This would require an anomalously high sedimentation rate of around 10 mm/yr, which is unlikely for this setting. Therefore, the preferred interpretation is that transgression took place in Marajó Island during expanding polar ice sheets probably due to the effect of tectonic subsidence (Fig. 5H).

A progressive increase in marine inflow contribution is recorded in the last 10,479 ¹⁴C yr B.P., suggesting a maximum transgression of the core site above 18 m depth. This interpretation is consistent with the overall rise in sea-level during the last interglacial period, when a barred lagoon system developed (Fig. 5G). The system, represented by facies association F, remained active throughout the Holocene, being ultimately replaced by the present Lake Arari (Fig. 5H). The presence of sediments with marine derived organic matter near the top (approximately 3 m from surface) of the core reveals that the establishment of this lake took place very recently.

9. Conclusion

Sediment core-based studies aiming to reconstruct Quaternary depositional environments may be improved by integrating facies analysis with $\delta^{13}\text{C}$, $\delta^{15}\text{N}$, and C/N. This type of approach is particularly important in helping to distinguish marine, continental, and mixed influences in transitional environments. Application of these techniques in a continuous core acquired in northeastern Marajó Island provided information to reconstruct, for the first time, the history of relative sea-level fluctuations in a northern Brazilian area during the last 50,000 yr. This effort has allowed an analysis of the evolution of the studied sedimentary succession within the context of global sea-level change and regional tectonics. The results showed that, despite the influence of eustatic fluctuations due to expansions and contractions of polar ice sheets, tectonic subsidence played a significant role in the creation of new accommodation space for the Late Pleistocene and Holocene sedimentation in this northern Brazilian passive margin.

Acknowledgments

This work was funded by FAPESP (Project # 004/15518-6), with the logistic contribution of the Goeldi Museum and the Mayor of the town of Santa Cruz do Arari. The first and second authors hold a scholarship from FAPESP (Process # 2005/01816-8), and a research grant from CNPq (Process # 300739/2005-2), respectively. The authors thanked Dr. Nils-Axel Mörner and, in particular, Dr. Graham Wilson, for the numerous comments and suggestions that helped to significantly improve the first version of the manuscript.

References

- Adams, J.M., Faure, H., Faure-Denard, L., McGlade, J.M., Woodward, F.I., 1990. Increases in terrestrial carbon storage from the Last Glacial Maximum to the present. *Nature* 348, 11–14.
- Allen, J.R.L., 1982. *Sedimentary Structures: Their Character and Physical Basis*. Elsevier, Amsterdam, 663 p.
- Andrews, J.E., Greenway, A.M., Dennis, P.F., 1998. Combined carbon isotope and C/N ratios as indicators of source and fate of organic matter in a poorly flushed, tropical estuary: Hunts Bay, Kingston Harbour, Jamaica. *Estuarine, Coastal and Shelf Science* 46, 743–756.
- Arens, N.C., Jahren, A.H., Amundson, R., 2000. Can C3 plants faithfully record the carbon isotopic composition of atmospheric carbon dioxide? *Paleobiology* 26, 137–164.
- Atchley, S.C., Nordt, L.C., Dworkin, S.I., 2004. Eustatic control on alluvial sequence stratigraphy: a possible example from the Cretaceous–Tertiary transition of the Tornillo Basin, Big Bend National Park, west Texas, U.S.A. *Journal of Sedimentary Research* 74, 391–404.
- Azevedo, R.P., 1991. *Tectonic Evolution of Brazilian Equatorial Continental Margin Basins*. Ph.D. Thesis, Royal School of Mines Imperial College, London.
- Behling, H., 2002. Carbon storage increases by major forest ecosystems in tropical South America since the Last Glacial Maximum and the early Holocene. *Global and Planetary Change* 33, 107–116.
- Bordovskiy, O.K., 1965. Accumulation and transformation of organic substances in marine sediment. *Marine Geology* 3, 3–114.
- Chen, F., Zhang, L., Yang, Y., Zhang, D., 2008. Chemical and isotopic alteration of organic matter during early diagenesis: evidence from the coastal area off-shore the Pearl River estuary, south China. *Journal of Marine Systems* 74, 372–380.
- Chivas, A.R., Garcia, A., van der Kaars, S., Couapel, M.J.J., Holt, S., Reeves, J.M., Wheeler, D.J., Switzer, A.D., Murray-Wallace, C.V., Banerjee, D., Price, D.M., Wang, S.X., Pearson, G., Edger, N.T., Beaufort, L., De Deckker, P., Lawson, E., Cecil, C.B., 2001. Sea-level and environmental changes since the last interglacial in the Gulf of Carpentaria, Australia: an overview. *Quaternary International* 83–85, 19–46.
- Costa, J.B.S., Hasui, Y., 1997. Evolução geológica da Amazônia. In: Costa, M.L., Angélica, R.S. (Eds.), *Contribuições à Geologia da Amazônia*. In Sociedade Brasileira de Geologia, Belém, Brazil, pp. 15–19.
- Costa, J.B.S., Bemerguy, R.L., Hasui, Y., Borges, M.S., 2001. Tectonics and paleogeography along the Amazon River. *Journal of South American Earth Sciences* 14, 335–347.
- Costa, J.B., Hasui, Y., Bemerguy, R.L., Soares-Júnior, A.V., Villegas, J., 2002. Tectonics and paleogeography of the Marajó Basin, northern Brazil. *Anais da Academia Brasileira de Ciências* 74, 519–531.
- Cloern, J.E., Canuel, E.A., Harris, D., 2002. Stable carbon and nitrogen isotope composition of aquatic and terrestrial plants of the San Francisco Bay estuarine system. *Limnology and Oceanography* 47, 713–729.
- Crowley, T.J., North, G.R., 1991. *Paleoclimatology*. Oxford University Press, New York.
- Dalrymple, R.W., 2006. Incised valleys in time and space: introduction to the volume and an examination of the controls on valley formation and filling. In: Dalrymple, R.W., Leckie, D.A., Tillman, R. (Eds.), *Incised Valleys in Time and Space: SEPM Special Publication*, vol. 85, pp. 5–12.
- Dalrymple, R.W., Zaitlin, B.A., Boyd, R., 1992. Estuarine facies models: conceptual basis and stratigraphic implications. *Journal of Sedimentary Petrology* 62, 1130–1146.
- Dalrymple, R.W., Boyd, R., Zaitlin, B.A., 1994. *Incised-Valley Systems: Origin, and Sedimentary Sequences: SEPM, Special Publication* 51, p. 399.
- Dalrymple, R.W., Leckie, D.A., Tillman, R., 2006. *Incised valleys in time and space*. SEPM Special Publication 85, Oklahoma.
- Deines, P., 1980. The isotopic composition of reduced organic carbon. In: Fritz, P., Fontes, J.C. (Eds.), *Handbook of Environmental Isotope Geochemistry*. Gisewir, Amsterdam.
- Fenies, H., Faugères, J.C., 1998. Facies and geometry of tidal channel-fill deposits (Arcachon Lagoon, SW France). *Marine Geology* 150, 131–148.
- Frey, R.W., Pemberton, S.G., 1984. Trace fossil facies models. In: Walker, R.G. (Ed.), *Facies Models: Geoscience Canada Reprint Series*, vol. 1, pp. 189–207.
- Frey, R.W., Howard, J.D., 1986. Mesotidal estuarine sequences: a perspective from the Georgia Bight. *Journal of Sedimentary Petrology* 56, 911–924.
- Fry, B., Jannasch, H.W., Molyneux, S.J., Wirsen, C.O., Muramoto, J.A., King, S., 1991. Stable isotope study of the carbon, nitrogen and sulfur cycles in the Black Sea and the Cariaco Trench. *Deep-Sea Research* 38, 1003–1019.
- Goñi, M.A., Teixeira, M.J., Perkey, D.W., 2003. Sources and distribution of organic matter in a river-dominated estuary (Winyah Bay, SC, USA). *Estuarine, Coastal and Shelf Science* 57, 1023–1048.
- Haines, E.B., 1976. Stable carbon isotope ratios in biota, soils and tidal water of a Georgia salt marsh. *Estuarine and Coastal Marine Science* 4, 609–616.
- Hofmann, M., Broecker, W.S., Lynch-Stieglitz, J., 1999. Influence of a $[\text{CO}_2(\text{aq})]$ dependent biological C-isotope fractionation on glacial $^{13}\text{C}/^{12}\text{C}$ ratios in the oceans. *Global Biochemical Cycles* 13, 873–883.
- Hunt, J.M., 1970. The significance of carbon isotope variations in marine sediments. In: Hobson, G.D., Spears, G.C. (Eds.), *Advances in Organic Geochemistry*. Pergamon, Oxford, pp. 27–35.
- Ishiwatari, R., Usaki, M., 1987. Diagenetic changes of lignin compounds in a more than 0.6 million-year-old lacustrine sediment (Lake Biwa, Japan). *Geochimica et Cosmochimica Acta* 51, 321–328.
- Jasper, J.P., Gagosian, R.B., 1990. The sources and deposition of OM in the late Quaternary Pigmy Basin, Gulf of Mexico. *Geochimica et Cosmochimica Acta* 54, 1117–1132.
- Keil, R.G., Tsamakis, E., Fuh, C.B., Giddings, J.C., Hedges, J.I., 1994. Mineralogical and textural controls on organic composition of coastal marine sediments: hydrodynamic separation using SPLITT fractionation. *Geochimica et Cosmochimica Acta* 57, 879–893.
- Lamb, A.L., Wilson, G.P., Leng, M.J., 2006. A review of coastal palaeoclimate and relative sea-level reconstructions using $\delta^{13}\text{C}$ and C/N ratios in organic material. *Earth-Science Reviews* 75, 29–57.
- Lehmann, M.F., Bernasconi, S.M., Barbieri, A., McKenzie, J.A., 2002. Preservation of organic matter and alteration of its carbon and nitrogen isotope composition during simulated and in situ early sedimentary diagenesis. *Geochimica et Cosmochimica Acta* 66, 3573–3584.
- Martino, R.L., 1996. Stratigraphy and depositional environments of the Kanawha Formation (Middle Pennsylvanian), southern West Virginia, U.S.A. *International Journal of Coal Geology* 31, 217–248.
- Martino, R.L., Sanderson, D.D., 1993. Fourier and autocorrelation analysis of estuarine tidal rhythmites, lower Breathitt Formation, eastern Kentucky, USA. *Journal of Sedimentary Petrology* 63, 105–119.
- McLaurin, B.T., Steel, R.J., 2007. Architecture and origin of an amalgamated fluvial sheet sand, lower Castlegate Formation, Book Cliffs, Utah. *Sedimentary Geology* 197, 291–311.

- Meyers, P.A., 1994. Preservation of elemental and isotopic source identification of sedimentary organic matter. *Chemical Geology* 114, 289–302.
- Meyers, P.A., 1997. Organic geochemical proxies of paleoceanographic, paleolimnologic, and paleoclimatic processes. *Organic Geochemistry* 27, 213–250.
- Middelburg, J.J., Nieuwenhuize, J., 1998. Carbon and nitrogen stable isotopes in suspended matter and sediments from the Schelde Estuary. *Marine Chemistry* 60, 217–225.
- Miotto J.A., 1993. Sismicidade e zonas sísmicas do Brasil. Doctoral Thesis. Universidade Estadual Paulista, Rio Claro, Brazil.
- Müller, A., 2001. Late- and Postglacial sea-level change and palaeoenvironments in the Oder Estuary, Southern Baltic Sea. *Quaternary Research* 55, 86–96.
- Nakatsuka, T., Handa, N., Harada, N., Sugimoto, T., Imaizumi, S., 1997. Origin and decomposition of sinking particulate organic matter in the deep water column inferred from the vertical distributions of its $\delta^{15}\text{N}$, $\delta^{13}\text{C}$ and $\delta^{14}\text{C}$. *Deep-Sea Research* 44, 1957–1979.
- Newman, J.W., Parker, P.L., Behrens, E.W., 1973. Organic carbon isotopic ratios in Quaternary cores from the Gulf of Mexico. *Geochimica et Cosmochimica Acta* 37, 225–238.
- Nichols, G.J., Fisher, J.A., 2007. Processes, facies and architecture of fluvial distributary system deposits. *Sedimentary Geology* 195, 75–90.
- Nilsen, T.H., McLaughlin, R.J., 1985. Comparison of tectonic framework and depositional patterns of the Hornelen strike-slip basin of Norway and the Ridge and Little Sulphur Creek strike slip-basins of California. In: Biddle, K.T., Christie-Blick, N. (Eds.), *Strike-slip deformation, basin formation and sedimentation: SEPM Special Publication*, vol. 37, pp. 79–103.
- O' Leary, M.H., 1988. Carbon isotopes in photosynthesis. *Bioscience* 38, 328–336.
- Peterson, B.J., Howarth, R.W., 1987. Sulfur, carbon, and nitrogen isotopes used to trace organic matter flow in the salt-marsh estuary of Sapelo Island, Georgia. *Limnology and Oceanography* 32, 1195–1213.
- Peterson, B.J., Fry, B., Hullar, M., Saupe, S., Wright, R., 1994. The distribution and stable carbon isotope composition of dissolved organic carbon in estuaries. *Estuaries* 17, 111–121.
- Prahl, F.G., Bennet, J.T., Carpenter, R., 1980. The early diagenesis of aliphatic hydrocarbons and organic matter in sedimentary particles from Dabob Bay, Washington. *Geochimica et Cosmochimica Acta* 44, 1967–1976.
- Prahl, F.G., Ertel, J.R., Goñi, M.A., Sparrow, M.A., Eversmeyer, B., 1994. Terrestrial organic carbon contributions to sediments on the Washington margin. *Geochimica et Cosmochimica Acta* 58, 3035–3048.
- Premuzic, E.T., Benkovitz, C.M., Gaffney, J.S., Walsh, J.J., 1982. The nature and distribution of organic matter in the surface sediments of world oceans and seas. *Organic Geochemistry* 4, 63–77.
- Raymond, P.A., Bauer, J.E., 2001. Use of ^{14}C and ^{13}C natural abundances for evaluating riverine, estuarine, and coastal DOC and POC sources and cycling: a review and synthesis. *Organic Geochemistry* 32, 469–485.
- Rossetti, D.F., Valeriano, M.M., 2006. Evolution of the lowest Amazon basin modeled from the integration of geological and SRTM topographic data. *Catena* 70, 253–265.
- Rossetti, D.F., Valeriano, M.M., Thallés, M., 2007. An abandoned estuary within Marajó Island: implications for late quaternary paleogeography of northern Brazil. *Estuaries and Coasts* 30, 813–826.
- Rossetti, D.F., Valeriano, M.M., Góes, A.M., Thalles, M., 2008a. Palaeodrainage on Marajó Island, northern Brazil, in relation to Holocene relative sea-level dynamics. *The Holocene* 18, 923–934.
- Rossetti, D.F., Góes, A.M., Valeriano, M.M., Miranda, M.C.C., 2008b. Quaternary tectonics in a passive margin: Marajó Island, northern Brazil. *Journal of Quaternary Science* 23, 121–135.
- Ruttenberg, K.C., Göni, M.A., 1997. Phosphorus distribution, C:N:P ratios, and $\delta^{13}\text{C}$ in arctic, temperate and tropical coastal sediments: tools for characterizing bulk sedimentary organic matter. *Marine Geology* 139, 123–145.
- Sachs, J.P., Repeta, D.J., 1999. Oligotrophy and nitrogen fixation during eastern Mediterranean sapropel events. *Science* 286, 2485–2488.
- Salomons, W., Mook, W.G., 1981. Field observations of the isotopic composition of particulate organic carbon in the southern North Sea and adjacent estuaries. *Marine Geology* 41, 11–20.
- Saino, T., Hattori, A., 1980. ^{15}N natural abundances in oceanic suspended particulate matter. *Nature* 283, 752–754.
- Schidlowski, M., Hayes, J.M., Kaplan, I.R., 1983. Isotopic inferences of ancient biochemistries: carbon, sulphur, hydrogen and nitrogen. In: Scholf, J.W. (Ed.), *Earth's Earliest Biosphere, its Origin and Evolution*: Princeton University Press, Princeton, pp. 149–186.
- Schleser, G.H., 1995. Parameters determining carbon isotope ratios in plants. In: Frenzel, B., Stauffer, B., Weib, M. (Eds.), *Problems of Stable Isotopes in Tree-Rings, Lake Sediments and Peat Bogs as Climate Evidence for the Holocene*: Fischer Verlag, Stuttgart, pp. 71–96.
- Sherr, E.B., 1982. Carbon isotope composition of organic seston and sediments in a Georgia salt marsh estuary. *Geochimica et Cosmochimica Acta* 46, 1227–1232.
- Sifeddine, A., Marint, L., Turcq, B., Volkmer-Ribeiro, C., Soubiès, F., Cordeiro, R.C., Suguio, K., 2001. Variations of the Amazonian rainforest environment: a sedimentological record covering 30,000 years. *Palaeogeography, Palaeoclimatology, Palaeoecology* 168, 221–235.
- St-Onge, G., Hillaire-Marcel, C., 2001. Isotopic constraints of sedimentary inputs and organic carbon burial rates in the Saguenay Fjord, Quebec. *Marine Geology* 176, 1–22.
- Street-Perrott, F.A., Ficken, K.J., Huang, Y., Eglinton, G., 2004. Late Quaternary changes in carbon cycling on Mt. Kenya, East Africa: an overview of the $\delta^{13}\text{C}$ record in lacustrine organic matter. *Quaternary Science Reviews* 23, 861–879.
- Szatmari, P., Fraçolin, J.B.L., Zanotto, O., Wolff, S., 1987. Evolução tectônica da margem equatorial brasileira. *Revista Brasileira de Geociências* 17, 180–188.
- Talma, A.S., Vogel, J.C., 1993. A simplified approach to calibrating ^{14}C dates. *Radiocarbon* 35, 317–322.
- Thompson, S., Eglinton, G., 1978. The fractionation of a recent sediment for organic geochemical analysis. *Geochimica et Cosmochimica Acta* 42, 199–207.
- Thornton, S.F., McManus, J., 1994. Applications of organic carbon and nitrogen stable isotope and C/N ratios as source indicators of organic matter provenance in estuarine systems: evidence from the Tay Estuary, Scotland. *Estuarine, Coastal and Shelf Science* 38, 219–233.
- Tyson, R.V., 1995. *Sedimentary Organic Matter: Organic Facies and Palynofacies*. Chapman & Hall, London.
- Van de Graaff, F.R., 1972. Fluvial-deltaic facies of the Castlegate Sandstone (Cretaceous), east-central Utah. *Journal of Sedimentary Petrology* 42, 558–571.
- Vital, H., 1988. Estudo do Geossistema do Lago Arari, Ilha de Marajó (PA). M.Sc. Thesis, Universidade Federal do Pará, Belém, Brazil.
- Westman, P., Hedenstrom, A., 2002. Environmental changes during isolation processes from the Litorina Sea as reflected by diatoms and geochemical parameters – a case study. *The Holocene* 12, 531–540.
- Wilson, G.P., Lamb, A.L., Leng, M.J., Gonzalez, S., Huddart, D., 2005. $\delta^{13}\text{C}$ and C/N as potential coastal palaeoenvironmental indicators in the Mersey Estuary, UK. *Quaternary Science Reviews* 24, 2015–2029.
- Zaitlin, B.A., Shultz, B.C., 1990. Wave-influenced estuarine sand body, Senlac heavy oil pool, Saskatchewan, Canada. In: Barwis, J.H., McPherson, J.G., Studlick, R.J. (Eds.), *Sandstone Petroleum Reservoirs*. Springer-Verlag, New York, pp. 363–387.
- Zaitlin, B.A., Dalrymple, R.W., Boyd, R., Leckie, D., 1994. The Stratigraphic Organization of Incised Valley Systems: Implications to hydrocarbon Exploration and Production – With Examples from the Western Canada Sedimentary Basin. Canadian Society of Petroleum Geologist, Calgary.
- Zaitlin, B.A., Warrern, M.J., Potocki, D., 2002. Depositional styles in a low accommodation foreland basin setting: an example from the Basal Quartz (Lower Cretaceous), southern Alberta. *Bulletin of Canadian Petroleum Geology* 50, 31–72.